PAPER • **OPEN ACCESS**

Synthesis and electrochemical performance of Li-rich xLi_2MnO_3•$(1-x)LiMn_{1/3}Ni_{1/3}Co_{1/3}O_2$ (x=0.2–0.5) cathode materials for lithium-ion batteries

To cite this article: L S Pechen *et al* 2019 *IOP Conf. Ser.: Mater. Sci. Eng.* **525** 012042

IOP Conf. Series: Materials Science and Engineering **525** (2019) 012042 doi:10.1088/1757-899X/525/1/012042

Synthesis and electrochemical performance of Li-rich $xLi_2MnO_3•(1-x)LiMn_{1/3}Ni_{1/3}Co_{1/3}O_2$ (x=0.2–0.5) cathode materials for lithium-ion batteries

L S Pechen[1], E V Makhonina[1], A M Rumyantsev[2,3], Yu M Koshtyal[2,3], A S Goloveshkin[4], V V Volkov[1], Yu A Politov[1] and I L Eremenko[1]

[1]N.S. Kurnakov Institute of General and Inorganic Chemistry, Russian Academy of Sciences, 31 Leninsky pr., Moscow, 119991 Russia
[2]Ioffe Institute, Russian Academy of Sciences, 26 Politekhnicheskaya, St Petersburg, 194021 Russia
[3]Peter the Great St.Petersburg Polytechnic University, 29 Polytechnicheskaya, St Petersburg, 195251 Russia
[4]Nesmeyanov Institute of Organoelement Compounds Russian Academy of Sciences, Russia, 28 Vavilova, Moscow, 119334 Russia

E-mail: lidia.s.maslennikova@gmail.com

Abstract. Li-excess transition metal oxides of the general composition $xLi_2MnO_3•(1-x)LiMO_2$ ($M=Mn_aNi_bCo_c$, a+b+c=1) are synthesized by coprecipitation method. Synthesis conditions for obtaining spherical particles with porous structure were determined. The influence of the oxide phase composition on their electrochemical performance as cathode materials is studied in lithium half-cells. All the samples show very high first-cycle coulombic efficiencies (more than 90%) in the voltage range of 2.5–4.8 V at a current density of 0.5*C*. It is reported that the Li-rich oxide of the composition $0.35Li_2MnO_3•0.65LiMn_{1/3}Ni_{1/3}Co_{1/3}O_2$ shows the better cycling performance in terms both discharge capacity and energy density and the best rate capability compared with the samples with larger and smaller contents of Li_2MnO_3.

1. Introduction

Currently, $LiCoO_2$, $LiNi_xCo_yMn_zO_2$, $LiMn_2O_4$, $LiNi_xCo_yAl_zO_2$, and $LiFePO_4$ are mainly used as positive electrode (cathode) materials for lithium–ion batteries (LIBs). However, the highest energy densities of these materials do not exceed 180–200 mA h/g. The development of high-energy cathode materials can significantly widen the LIB application. In addition, the cathode materials should have a good cyclability, be safe and not expensive.

Li-rich transition metal oxides have attracted attention as promising candidates for the new generation of cathode materials because of their high specific capacities [1, 2]. They can be written in two notations, $xLi_2MnO_3•(1-x)LiMO_2$ ($M=Mn_aNi_bCo_c$, a+b+c=1) or in the form with excessive lithium $Li_{(1+y)}M'_{(1-y)}O_2$ [1-3]. The first notation shows nanoscale inhomogeneity of these materials, because $LiMO_2$ (trigonal, R-3m) and Li_2MnO_3 (monoclinic, C2/m) have compatible oxygen lattices, allowing integration of the two structures. Up to now, the atomic structure of these materials is debated in the literature [4-8].

Li_2MnO_3 monoclinic phase is electrochemically inactive when cycled to 4.4 V. After activation to 4.5-4.8 V, there is observed a significant capacity increase that can be attributed to activation of the monoclinic phase. The activation involves delithiation and deoxidation processes and formation of electrochemically active $LiMnO_2$ phase [9-11]. The discharge capacities of Li-rich oxides can reach up to 250-300 mA h/g. However, the materials have a large first-cycle capacity loss and suffer from capacity fade and voltage decay during cycling. Despite the large body of research, Li-rich materials without the above drawbacks are not obtained till now because of the complexity of these structures.

In this work, we studied effect of the $Li_2MnO_3/LiMO_2$ phase composition in $xLi_2MnO_3•(1–x)LiMO_2$ Li-rich structures on their electrochemical characteristics. We choose the $LiMn_{1/3}Ni_{1/3}Co_{1/3}O_2$ composition of the trigonal phase as optimal that in terms of the electrochemical performance [12]. The oxides with 50, 35 and 20% of Li_2MnO_3 were synthesized.

2. **Experimental**

2.1. Synthesis procedure of Li-rich oxides

Li-rich oxides were synthesized by coprecipitation method followed by a solid-state reaction with $LiOH·H_2O$. The starting reagents were manganese nitrate tetrahydrate (98%, Alfa Aesar), nickel nitrate hexahydrate (99.9%, ABCR), cobalt nitrate hexahydrate (99% Acros Organics), sodium carbonate anhydrous (≥99%, Chimmed), ammonium hydroxide (special purity grade, Chimmed), and lithium hydroxide monohydrate (≥99%, Sigma-Aldrich). Solutions of metal nitrates (2 mol/L) and sodium carbonate (2 mol/L) with ammonium hydroxide (0.35 mol/L) were added dropwise in a quartz reactor partially filled with deionized water. Coprecipitation of carbonates MCO_3 ($M=Mn_xNi_yCo_z$) was carried out under CO_2 atmosphere.

The synthesis conditions of the carbonate precursors were optimized. The temperature was maintained at 60°C; solution pH was adjusted to 7.5, and the stirring speed fixed at 1000 rpm. Metal nitrates solution was added at a constant rate of about 120 mL/h. A Na_2CO_3/NH_3 solution was automatically added to maintain the solution pH at 7.5. The mature time was 12 h. Carbonate precursors prepared were thoroughly washed with deionized water, ethanol, and diethyl ether, and then dried at 120 °C at an argon atmosphere.

For solid-phase synthesis, appropriate amounts of lithium hydroxide monohydrate (with a 3% excess) and a precursor were thoroughly ground in an agate mortar and annealed at 480 (6 h) and 900°C (12 h). The mixture was repeatedly homogenized in the course of annealing. The samples containing 50, 35 and 20 % of Li_2MnO_3 phase ($0.5Li_2MnO_3•0.5LiMn_{1/3}Ni_{1/3}Co_{1/3}O_2$, $0.35Li_2MnO_3•0.65LiMn_{1/3}Ni_{1/3}Co_{1/3}O_2$ and $0.2Li_2MnO_3•0.8LiMn_{1/3}Ni_{1/3}Co_{1/3}O_2$) were prepared.

2.2. Material characterization

The powder X-ray diffraction (XRD) patterns were recorded using a Bruker D8 Advance diffractometer (Cu Kα radiation, λ=0.15418 nm, 45 kV/250 mA) at room temperature. The data were collected in the Θ/2Θ scan mode, 0.02° scan step in the 2 Θ range of 5°–80°. The precise X-ray analysis was carried out with a Bruker D8 Advance Vario (Cu Kα1) equipped with a Ge monochromator and position-sensitive detector LynxEye with rotating sample stage (the Θ/2Θ geometry). The data were collected with the use of the Bruker DIFFRACplus program package, the analysis was performed with the EVA and TOPAS programs.

Compositions of the resulting compounds were determined by inductively coupled plasma mass-spectrometry (ICP-MS) with an Agilent 7500ce system (”Agilent Technologies Inc.”).

The morphology and microstructure of the samples were studied by scanning electron microscopy (SEM) using a NVision-40 (Carl Zeiss) microscope.

Particle size analysis was performed with the use of a laser particle sizer Analysette 22 (Fritsch). We used the Fraunhofer model for data analysis.

2.3. Electrochemical tests

Electrochemical tests of the samples as cathode materials were carried out in CR2032 coin-type cells, using not less than 3 cells for each sample. The positive electrodes were prepared by mixing 92 wt% of an active material, 5 wt% of the conductive additive (Super C65, Timcal) and 3 wt% of polyvinylidene difluoride (Solef 5130, Solvay) in N-methyl-2-pyrrolidone. A mass load of active material in a cell was on average 8-12 mg. A lithium foil was used as anode and TC-E918 (Tinci) as the electrolyte.

The cells were cycled galvanostatically in different voltage ranges (50–300 cycles on average). Before the main electrochemical tests, all the cells were subjected to an activation stage. The activation stage included cycling in the voltage ranges of 2.5–4.2 V, 2.5–4.4 V, 2.5–4.8 V and again 2.5–4.4 V (two cycles for each range). Hereafter, if the sample showed an acceptable result, further studies in the required voltage ranges were performed. Rate capability of the Li-rich materials was also investigated in different voltage ranges. The charge current density was 10-100 mA/g, discharge current density was 10-1000 mA/g.

3. Results and discussions

Li-rich oxides containing 50, 35 and 20 % of Li_2MnO_3 phase ($0.5Li_2MnO_3 \bullet 0.5LiMn_{1/3}Ni_{1/3}Co_{1/3}O_2$, $0.35Li_2MnO_3 \bullet 0.65LiMn_{1/3}Ni_{1/3}Co_{1/3}O_2$ and $0.2Li_2MnO_3 \bullet 0.8LiMn_{1/3}Ni_{1/3}Co_{1/3}O_2$) prepared by the above procedure hereafter are denoted LRC50, LRC35, LRC20, respectively. The samples are black powders consisting of spherical agglomerates with narrow size distribution (Figure 1, Table 1).

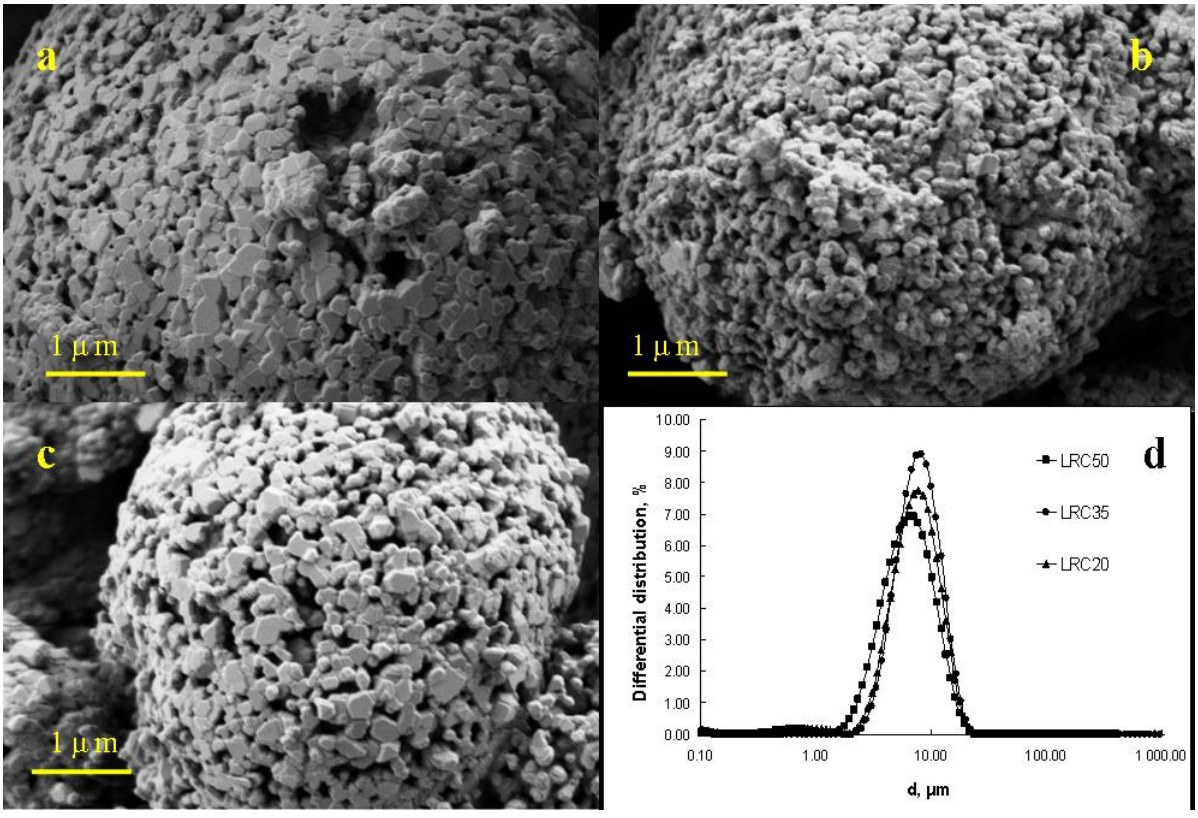

Figure 1. SEM images of samples (a) LRC50, (b) LRC35, and(c) LRC20; and (d) differential particle size distribution of the samples.

The agglomerate and primary particle sizes are close to each other for all the samples. The chemical compositions of the samples determined by ICP–MS analysis were found to be very close the target compositions (Table 1).

Table 1. Morphological characteristics of pristine Li-rich materials and data of ICP-MS analysis.

Sample	Primary particle size range, nm	Agglomerate size distribution, μm			ICP-MS data, at % (at.)			
		D10	D50	D90	Li	Mn	Ni	Co
LRC50	10-400	2.8	5.7	11.0	1.226	0.537	0.131	0.131
LRC35	100-300	4.1	7.3	12.4	1.138	0.483	0.186	0.193
LRC20	100-300	3.6	6.9	12.3	1.09	0.423	0.250	0.237

The XRD patterns of the samples with different $Li_2MnO_3/LiMO_2$ ratio are shown in Figure 2.

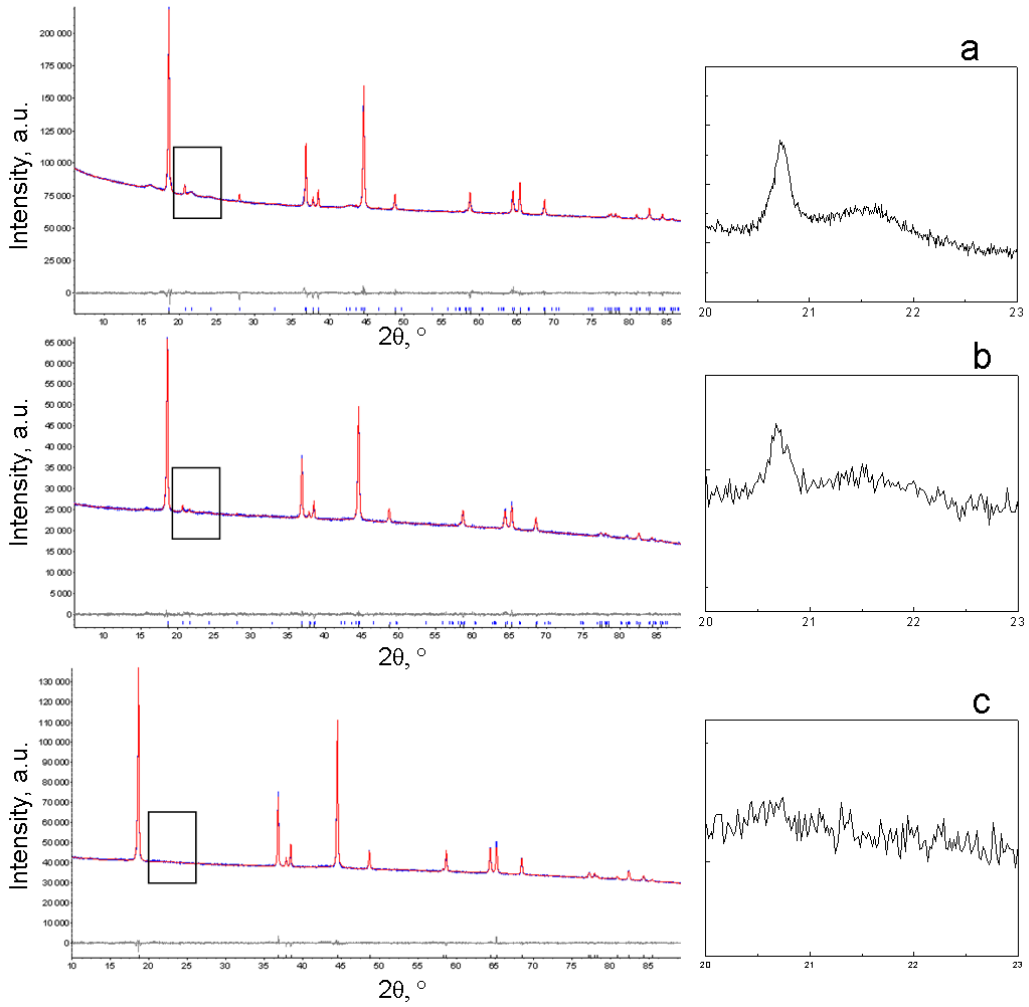

Figure 2. The Rietveld profile fittings of X-ray diffraction patterns of experimental (blue lines) and fitting (red lines) X-ray diffraction patterns of (a) LRC50, (b) LRC35, (c) LRC20 samples. The positions of Bragg reflections are denoted by vertical bars. The difference (experiment minus calculation) curve is shown by a gray line at the bottoms.

Most of the reflections can be indexed based on the trigonal R-3m structure. The small peaks between 20° and 23° (Figure 2, inserts) can be indexed in a monoclinic superstructure *C*2/*m* indicating

an ordering in the transition metal layer. Predictably, the intensities of these peaks decrease with decreasing Li_2MnO_3 content in the sample and practically vanish in the diffraction pattern of LRC20/80 sample. The crystallite sizes were estimated by Williamson-Hall method to be 50–70 nm for all the samples. The lattice parameters of the samples and coherent scattering lengths are summarized in Table 2. These values are lower than primary particle sizes observed by SEM (Table 1). Presumably, the particles can contain several crystallites or only a part of particle has a crystal structure.

Table 2. Lattice parameters of Li-rich samples.

Sample	a, Å	c, Å	V, Å3	Coherent scattering length, nm
LRC50	2.85177(3)	14.2371(3)	100.273(3)	56(1)
LRC35	2.85534(5)	14.2531(6)	100.634(6)	63(1)
LRC20	2.85839(3)	14.2453(3)	100.796(3)	78(2)

Figure 3a,b shows discharge voltage profiles of the samples in 3-rd and 50-th cycles in the range of 2.5-4.8 V at a current density of 100 mA/g (C/2). The discharge capacities of all the samples in the 3rd cycle are close to each other, at the same time we observe a tendency to decreasing the discharge capacity in the row LRC50–LRC35–LRC20. The samples have high values of the first-cycle coulombic efficiency in this voltage range, namely, 90% for LRC50 and LRC20 and 92% for LRC35. These values of the first-cycle irreversible capacity loss are considerably lower than those usually reported in the literature [13, 14].

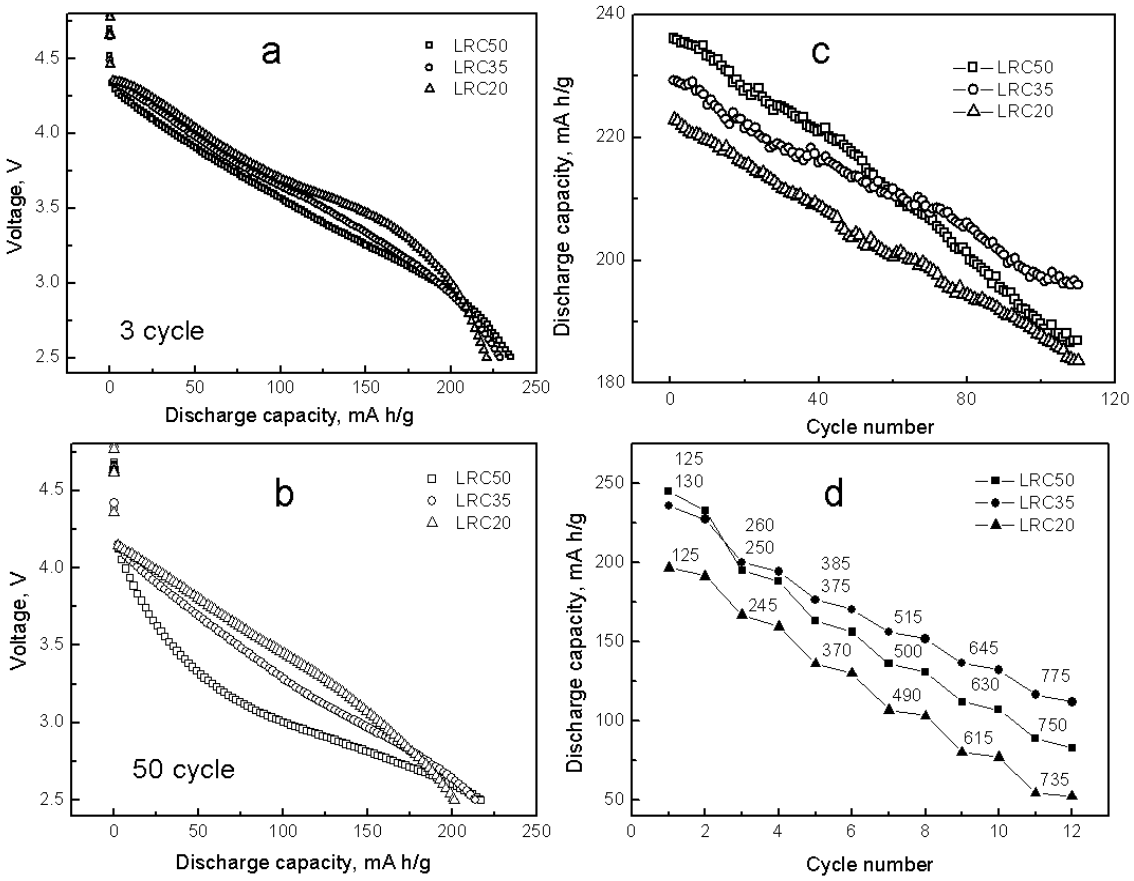

Figure 3. (a, b) Discharge voltage profiles for the 3-rd and 50-th cycles, respectively, for the samples in the voltage range of 2.5-4.8 V at a current density of 100 mA/g; (c) cycling behavior of the samples at a current density of 100 mA/g; and (d) the rate capability of the samples in the range of 2.5-4.8 V (current densities (mA/g) at the each step are shown in the figure).

In Figure 3c, we demonstrate cycling behavior of all the samples in the same voltage range of 2.5-4.8 V. As is seen, LRC35 sample is cycling better than other two samples. The capacity retention for this sample is 85% at the 110 cycle. The capacity retentions for LRC50 and LRC20 samples are 79% and 81%, respectively. LRC35 sample also shows the best rate capability (Figure 3d). The rate capabilities of the samples differ more considerably. The discharge capacity of LRC35 at the discharge current density of 775 mA/g is 47% from the initial discharge capacity at the current density of 125 mA/g, while the analogous values for LRC50 and LRC20 samples are 33 and 26%, respectively.

In the course of cycling, the average voltage of cells continuously decreases with each successive charge and discharge cycle. A serious voltage fade for these materials is generally considered to originate from the gradual structural transformation during cycling, mostly to a spinel-like structure [15-17] and appearing new low-voltage redox potentials. A new structure gradually formed undergoes, at least partially, reversible redox transformations [18, 19]. This process is related to the transition-metal (TM) ions migration from octahedral sites in the TM slabs to octahedral sites in the Li slabs through intermediary Li-slab tetrahedral sites in the course of lithiation/delithiation [18, 19].

The voltage fade is characteristic of all the samples synthesized, at the same time, the more the Li_2MnO_3 content, the more the voltage fade (Figure 3a). The values of the voltage fade at the 50th cycle are equal to 11.3, 7.3, and 6.2%, for LRC50, LRC35, and LRC20, respectively. To take into account this voltage decay, we compared the energy densities of the samples that characterize both specific discharge capacities and the discharge voltage. The energy densities for each cycle (E_n) were calculated as the integration areas under the corresponding discharge curves. The energy retentions for the 110-th cycle (E_{110}/E_3) are 63.1, 75.8, and 71.5% for samples LRC50, LRC35, and LRC20, respectively.

Therefore, the sample of the composition $0.35Li_2MnO_3 \cdot 0.65LiMn_{1/3}Ni_{1/3}Co_{1/3}O_2$ demonstrates a better electrochemical performance than the samples with both larger and smaller contents of the monoclinic phase.

4. Conclusion

In this work, we studied the effect of the phase composition in Li-rich complex oxides $xLi_2MnO_3 \cdot (1-x)LiMn_{1/3}Ni_{1/3}Co_{1/3}O_2$ obtained by coprecipitation method on their electrochemical behavior. All the samples show very high first-cycle coulombic efficiencies (equal to and more than 90%) in the voltage range of 2.5–4.8 V at a current density of 0.5*C*.

The Li-rich oxide of the composition $0.35Li_2MnO_3 \cdot 0.65LiMn_{1/3}Ni_{1/3}Co_{1/3}O_2$ (LRC35) shows the better cycling performance in terms both discharge capacity and energy density and the best rate capability compared with the samples with larger and smaller contents of Li_2MnO_3.

Acknowledgments

This work was supported by the Russian Science Foundation, Grant # 17-13-01424 (2017).

References

[1] Thackeray M M, Kang S H, Johnson C S, Vaughey J T, Benedek R and Hackney S A. 2007 *J. Mater. Chem.* **17** 3112–25
[2] Koga H, Croguennec L, Menetrier M, Douhil K, Belin S, Bourgeois L, Suard E, Weill F and Delmas C 2013 *J. Electrochem. Soc*. **160** A786–92
[3] Johnson C, Kim J, Lefief C, Vaughey J T and Thackeray M M 2004 *Electrochem. Commun*. **6** 1085–91
[4] Thackeray M M, Kang S H, Johnson C S, Vaughey J T and Hackney S A 2006 *Electrochem. Commun.* **8** 1531–38
[5] Croguennec L, Polacin M. R 2015 *J. Am. Chem. Soc*. **137** 3140–56
[6] Zheng J, Xu P, Gu M, Xiao J, Browning N D, Yan P, Wang C, Zhang J-G 2015 *Chem. Mater* **27** 1381–90

[7] Ohzuku T, Nagayama M, Tsuji K, Ariyoshi K 2011 *J. Mater. Chem.* **21** 10179–88
[8] Shukla A K, Ramasse Q M, Ophus C, Duncan H, Hage F and Chen G 2015 *Nature Comm.* **6** 8711
[9] Sathiya M, et al. 2013 *Nature Materials* **12** 827–35
[10] Roziera P and Tarascon J M 2015 *J. Electrochem. Soc.* **162** A2490–99
[11] Hy S, Liu H, Zhang M, Qian D, Hwang B-J and Meng Y S 2016 *Energy Environ. Sci.* **9** 1931
[12] Koyama Y, Makimura Y, Tanaka I, Adachi H and Ohzuku T 2004 *J. Electrochem. Soc.* **151** A1499–1506
[13] Mohanty D, Sefat A S, Li J, Meisner R A, Rondinone A J, Payzant E A, Abraham D P, Wood D L, Daniel C 2013 *Phys.Chem. Chem. Phys.***15** 19496-509
[14] Erikson E M, Schipper F, Penki T R, Shin J-Y, Erk C, Chesneau F-F, Markovsky B and Aurbach D 2017 *J. Electrochem. Soc*. **164** A6341–48
[15] Bettge M, Li Y, Gallagher K G, Zhu Y, Wu Q, Lu W, Bloom I and Abraham D P 2013 *J. Electrochem. Soc.* **160** A2046–55
[16] Yan P, et al 2015 *Nano Lett.* **15** 514–22
[17] Gallagher K G, Croy J R, Balasubramanian M, Bettge M, Abraham D P, Burell A K, Thackeray M M 2013 *Electrochem.Comm.* **33** 96–98
[18] Croy J R, Balasubramanian M, Gallagher K G and Burell A K 2015 *Acc. Chem. Res.* **48** 2813–21
[19] Croy J R, Gallagher K G Balasubramanian M, Long B R and Thackeray M M 2014 *J. Electrochem. Soc* **25** A318–25